doi:10.1016/j.jmb.2004.08.054 J. Mol. Biol. (2004) 343, 659–670

JMB

Available online at www.sciencedirect.com

SCIENCE DIRECT®

ELSEVIER

Structural Analysis of *Arabidopsis thaliana* Nucleoside Diphosphate Kinase-2 for Phytochrome-mediated Light Signaling

Young Jun Im[1]†, Jeong-Il Kim[2,3]†, Yu Shen[4], Young Na[1], Yun-Jeong Han[4] Seong-Hee Kim[2,3], Pill-Soon Song[2,3,4]* and Soo Hyun Eom[1]*

[1]*Department of Life Science Gwangju Institute of Science and Technology, Gwangju 500-712, South Korea*

[2]*Environmental Biotechnology National Core Research Center Gyeongsang National University, Jinju 660-701 South Korea*

[3]*Kumho Life & Environmental Science Laboratory, 1 Oryong-Dong, Gwangju 500-712, South Korea*

[4]*Department of Chemistry University of Nebraska-Lincoln NE 68588-0304, USA*

**Corresponding authors*

In plants, nucleoside diphosphate kinases (NDPKs) play a key role in the signaling of both stress and light. However, little is known about the structural elements involved in their function. Of the three NDPKs (NDPK1–NDPK3) expressed in *Arabidopsis thaliana*, NDPK2 is involved in phytochrome-mediated signal transduction. In this study, we found that the binding of dNDP or NTP to NDPK2 strengthens the interaction significantly between activated phytochrome and NDPK2. To better understand the structural basis of the phytochrome–NDPK2 interaction, we determined the X-ray structures of NDPK1, NDPK2, and dGTP-bound NDPK2 from *A. thaliana* at 1.8 Å, 2.6 Å, and 2.4 Å, respectively. The structures showed that nucleotide binding caused a slight conformational change in NDPK2 that was confined to helices αA and α2. This suggests that the presence of nucleotide in the active site and/or the evoked conformational change contributes to the recognition of NDPK2 by activated phytochrome. *In vitro* binding assays showed that only NDPK2 interacted specifically with the phytochrome and the C-terminal regulatory domain of phytochrome is involved in the interaction. A domain swap experiment between NDPK1 and NDPK2 showed that the variable C-terminal region of NDPK2 is important for the activation by phytochrome. The structure of *Arabidopsis* NDPK1 and NDPK2 showed that the isoforms share common electrostatic surfaces at the nucleotide-binding site, but the variable C-terminal regions have distinct electrostatic charge distributions. These findings suggest that the binding of nucleotide to NDPK2 plays a regulatory role in phytochrome signaling and that the C-terminal extension of NDPK2 provides a potential binding surface for the specific interaction with phytochromes.

Keywords: Arabidopsis; nucleoside diphosphate kinase; phytochrome

Introduction

Nucleoside diphosphate kinases (NDPKs; EC2.7.4.6) are ubiquitous housekeeping enzymes that catalyze the transfer of a γ-phosphoryl group from a nucleoside triphosphate (NTP) to a nucleoside diphosphate (NDP).[1] Previous studies of NDPKs have revealed in detail the catalytic mechanism of the phosphotransfer reaction.[2–5] The enzyme functions *via* a ping-pong mechanism in which it is transiently phosphorylated by a donor NTP on a histidine residue conserved in all NDPKs. After release of the donor, an acceptor NDP binds at the same site and receives the phosphoryl group to yield the NTP product. A number of crystal

† Y.J.I. & J.-I.K. contributed equally to this work.

Abbreviations used: NDPK, nucleoside diphosphate kinase; Pr, red-light-absorbing form of phytochrome; Pfr, far-red-light-absorbing form of phytochrome; phyA, phytochrome A; PΦB, phytochromobilin; GST, glutathione-*S*-transferase; PVDF, polyvinylidene difluoride; Ab, antibody; mAb, monoclonal antibody; PAS, Per/Arnt/Sim (period clock protein/aryl hydrocarbon receptor nuclear translator/single-minded protein).

E-mail addresses of the corresponding authors: eom@gist.ac.kr; pssong@kkpc.com

structures of NDPKs from both animals and prokaryotes have been reported.[6–14] The eukaryotic enzymes are homohexamers, whereas several of the prokaryotic enzymes are homotetramers.[15] Whether tetramer or hexamer, the NDPK active sites are structurally identical, and almost all the residues involved in the active site are fully invariant from bacteria to humans.[16] Interestingly, despite the fact that they share highly conserved enzymatic functions and structures, NDPKs exhibit diverse regulatory functions that may be related to, or independent of, their catalytic activity.[17–20] For instance, NM23-H1, a human NDPK-A acts as a transcription factor suppressing metastasis in carcinoma cell lines and as a DNase in cytotoxic T-lymphocyte-induced apoptosis.[21,22] Although there is abundant evidence for these additional regulatory functions of NDPKs, their respective molecular mechanisms are not yet well understood.

In plants, NDPKs are involved in responses to heat stress,[23] UV-B light signaling,[24] growth,[25] reactive oxygen species signaling,[26] and phytochrome signaling.[27] *Arabidopsis thaliana* expresses three NDPKs, NDPK1, NDPK2 and NDPK3 (GenBank accession numbers AF017641, AF017640, and AF044265, respectively), among which only NDPK2 reportedly interacts with phytochromes, the molecular light switches that mediate the transcriptional regulation of the plant's growth and development.[28–30] These chromoproteins exist as homodimers with covalently linked tetrapyrrole chromophore, called phytochromobilin, which occur as two photo-interconvertible species: the red light-absorbing Pr form and the far red light-absorbing Pfr form. The Pfr form is considered the active form of phytochrome because of the promotive effect of red light on most of the plant's physiological responses. NDPK2 is catalytically activated in the presence of Pfr phytochromes and appears to exert a positive effect on cotyledon unfolding and greening responses elicited by light and phytochromes.[27] Thus, *Arabidopsis* NDPK2 is likely a positive signaling component of phytochrome-mediated signal transduction pathways. However, why NDPK2 interacts specifically with phytochromes, and how its interaction mediates signaling, remains unclear.

To better understand the structural basis for the specific recognition of NDPK2 by phytochrome, we determined the crystal structures of NDPK1, NDPK2, and dGTP-bound NDPK2 from *A. thaliana* and examined the nucleotide-dependent interaction of the proteins and the binding region of NDPK2 in phytochrome using *in vitro* binding assays.

Results

Interaction of NDPK2 with phytochromes

We previously reported that NDPK2 was activated *via* interaction with the Pfr form of phyA, though the interaction was usually weak.[27] To determine the conditions under which the interaction would be stronger, in the present study we evaluated the binding in the presence of dNDP or NTP by *in vitro* binding assays under the conditions used earlier. The Pr or Pfr form of phyA used for the assay was prepared by illuminating the samples with far-red or red light. Interestingly, the interaction of phyA and NDPK2 was dependent on the presence of dCDP or ATP (Figure 1A). The relative intensity of the Pfr form interacting with NDPK2 in the presence of ATP or dCDP was about six times higher than the Pr form in the absence of nucleotide, and three times higher than the Pr form in the presence of nucleotides. The interaction of NDPK2 to Pfr forms of phyA was dependent on the concentration of dCDP with the maximum affinity around 2 mM dCDP (Figure 1B). In other words, in the absence of dCDP or ATP, NDPK2 binding to phyA, even to the Pfr form, remained weak. That it was strengthened significantly by addition of dCDP or ATP indicates NDPK2 interacts with phyA mainly after being loaded with dNDP or NTP.

We also had previously used yeast two-hybrid screening to show that, among the three *Arabidopsis* NDPKs, only NDPK2 interacts specifically with phytochromes.[27] In the present study, we confirmed the specific recognition of NDPK2 by phyA in immunoprecipitation assays (Figure 1C). After incubating the Pfr form of phyA and each isoform of GST-NDPKs in the presence of 2 mM dCDP, protein A/G beads were added. The harvested beads were washed and analyzed in Western blots probed with anti-oat phyA and anti-GST mAbs (Oncogene). Among three NDPK isoforms, only NDPK2 interacted with phyA. The sequence alignment of NDPK isoforms reveals that they share 72–75% similarity with variable residues mostly within the C-terminal 30 amino acid residue extension, implying a potential contribution of the C-terminal extension for the specificity of the interaction (Figure 1D).

We next determined the binding regions of NDPK2 in phytochrome by examining the interactions with various deletion mutants of phytochrome. Phytochromes are composed of several domains known as an N-terminal extension (amino acid residues 1–65) that undergoes conformational change upon phototransformation, an N-terminal chromophore lyase domain (1–407) for chromophore attachment, Per/Arnt/Sim (PAS)-related domains (611–870), and a histidine kinase-related domain (871–1192).[31–33] We initially constructed several phyA deletion mutants lacking the N or C terminus (Figure 2A). Assembly of the full-length (1–1129), A957 (1–957), A407 (1–407), AΔ65 (66–1129), and AC (574–1129) constructs into holophytochromes was verified by Zn blot analysis (Figure 2B), and the proteins showed the appropriate Pr/Pfr spectra of phyA (data not shown). Interactions between phyA constructs and NDPK2 were then confirmed by *in vitro* binding assays and immunoprecipitation (Figure 2C). The results showed that the full-length protein, A957, AΔ65 and AC mutants all interacted

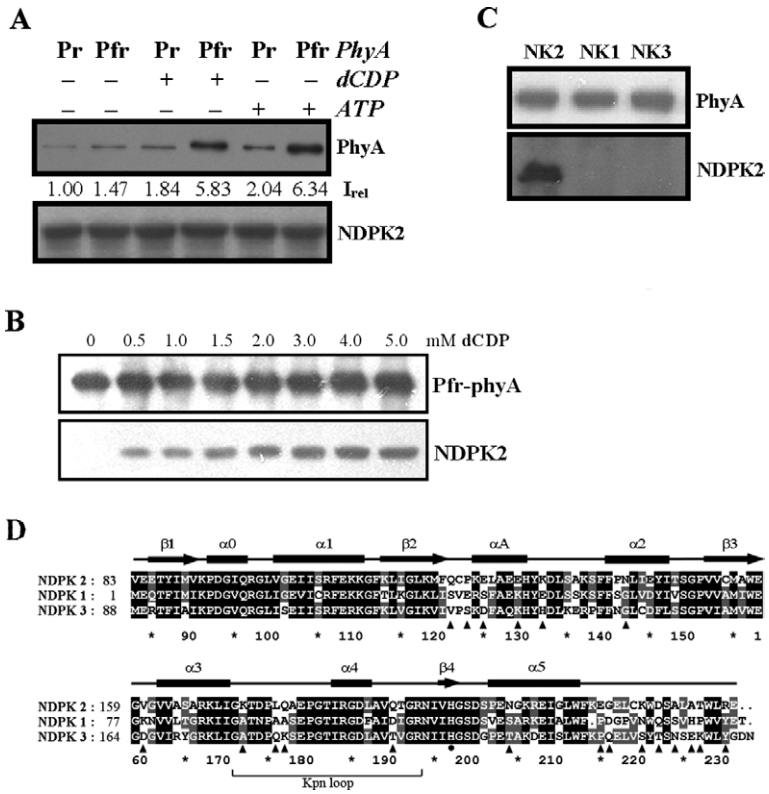

Figure 1. *In vitro* assays of interaction between phyA and NDPKs. A, Pull-down assays carried out in the absence or presence of dNDP/NTP. A mixture of GST-NDPK2 and phyA were incubated then harvested with glutathione resin, after which Western blot analysis was performed. The interaction was increased significantly only for the Pfr form of phyA and only in the presence of dCDP or ATP. I_{rel} are the relative signal intensities under the indicated conditions; the signal obtained in the first lane (Pr + NDPK2 in the absence of dCDP or ATP) was assigned a value of 1.00. B, Pull-down assays showing the interaction of NDPK2 and the Pfr forms of phyA under different concentrations of dCDP. C, Immunoprecipitation assays illustrating the interaction between phyA and NDPK2. Pfr forms of phyA and anti-oat phyA mAb (oat22) were used for the assay. Among the three NDPK isoforms, only NDPK2 interacted with phyA. D, Sequence alignment of *Arabidopsis thaliana* NDPK isoforms. The secondary structural elements are indicated with bars and arrows. The signal sequences of NDPK1 and NDPK3 were not included in the alignment. The histidine residue in the active site is indicated by a filled circle. The variable residues that differ from NDPK2 are indicated by filled triangles. Sequence alignment was generated by CLUSTAL_X.[53]

with NDPK2, whereas the A407 mutant did not. This means that a region extending from residues 574 to 957 of phyA interacts with NDPK2, which is consistent with our earlier findings that two missense mutations (G765D and G788E) in the PAS domain disrupted the interaction with NDPK2 by using yeast two-hybrid methods and the C-terminal regulatory domain of phytochrome is sufficient for the interaction with NDPK2.[27]

From the sequence alignment of NDPK1 and NDPK2 (Figure 1D), most variable residues occur in the C-terminal 30 residue region. To confirm the importance of this domain for the binding with phytochrome, we performed a domain-swap experiment using NDPK1 and NDPK2 (Figure 3A). Since NDPK2 activation by phytochromes requires physical interaction with phytochromes and follows Michaelis–Menten kinetics with a specific K_m value,[27] we checked the NDPK γ-phosphate exchange activities in the presence of Pfr phytochrome with domain-swap mutants, NK21 (NDPK2 containing the C-terminal extension of NDPK1) and NK12 (NDPK1 containing the C-terminal extension of NDPK2) (Figure 3A). NDPK2 could be activated by addition of the Pfr form of phytochrome and had higher γ-phosphate exchange activity than NDPK1, while NDPK1 showed little activation by phytochrome (Figure 3B).

When the domain-swapped mutants were tested, NK12 was activated significantly by phyA but NK21 showed little activation by phyA, similar to NK1 (Figure 3C). The domain swap mutants, NK12 and NK21 have much lower enzymatic activities, especially compared to NDPK2, probably due to the disruption of ideal conformation of active-site residues by X mutations. The N-terminal part of NDPK usually determines the enzymatic activity, but the C-terminal part is also involved, especially residues in the α4 helix such as Ser199 and E208. They form the H-bonding with His197. If the domains were swapped, the H-bonding with the His residue would not be ideal for NDPK enzymatic activity. Therefore, NK12 and NK21 might not possess ideal arrangement of active sites, showing much lower enzymatic activities. Though the activity of the NK12 mutant is not comparable to

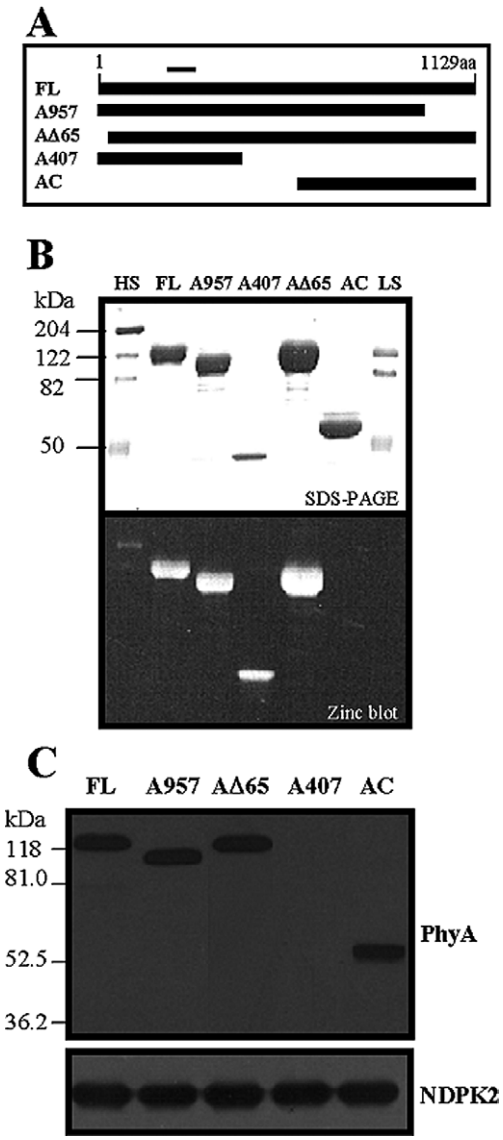

Figure 2. The NDPK2 binding region of phyA. A, A representation of the phyA deletion mutants used: FL, full-length oat phyA (amino acid residues 1–1129); A957, C-terminal deleted phyA (1–957); AΔ65, N-extension-deleted phyA (66–1129); A407, N-terminal domain of phyA (1–407); AC, C-terminal domain of phyA (574–1129). The small bar at the top indicates the chromophore-binding site. B, SDS-PAGE of purified phyA and its deletion mutants (upper panel) and their Zn blots (lower panel): lane HS, high molecular mass protein markers (Bio-Rad); lane LS, low molecular mass protein markers (Bio-Rad). C, Pull-down assays using NDPK2 and the Pfr forms of the indicated phyA deletion mutants. The C-terminal domain of phyA (AC) was sufficient for the interaction; deletion of the N-terminal extension (residues 1–65) or the C-terminal region (958–1129) did not affect the interaction.

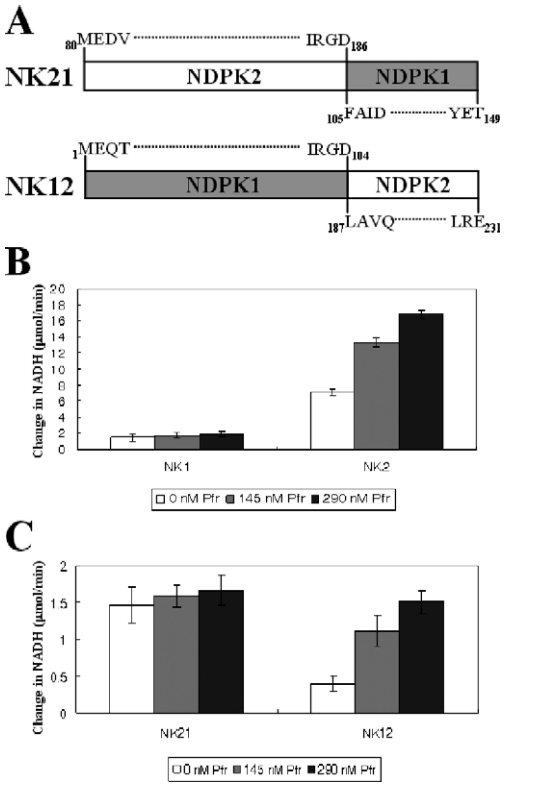

Figure 3. The γ-phosphate exchange activity of domain-swapped NDPK mutants. A, Domain structure of the domain-swap mutants between NDPK1 and NDPK2. In all, 45 residues in the C-terminal domain of both NDPKs were switched. Mutant NK21 contains the N-terminal domain of NDPK2 and the C-terminal domain of NDPK1, whereas mutant NK12 contains the N-terminal domain of NDPK1 and the C-terminal domain of NDPK2. B, The stimulation of the γ-phosphate exchange activities of NDPK1 and NDPK2 by the Pfr form of oat phyA. Only NDPK2 is activated by phytochrome in a concentration-dependent manner. C, The stimulation of the γ-phosphate exchange activities of domain swap mutants by the Pfr form of oat phyA. Mutant NK12, which contains the C-terminal domain of NDPK2, was stimulated by the Pfr form of oat phyA significantly, whereas mutant NK21 was little stimulated by the Pfr form of phyA.

that of wild-type NDPK2, the significant activation of NK12 by the phytochrome as wild-type NDPK2 suggests that the C-terminal region of NDPK2 is important for the binding with phytochrome.

Overall structure of *Arabidopsis* NDPK2

To better understand the structural basis of the interaction between NDPK2 and phyA, we determined the crystal structures of *A. thaliana* NDPK1 and NDPK2. We found that the enzymes form hexamers very similar to other eukaryotic NDPKs (Figure 4A). The six independent subunits in the asymmetric unit were virtually identical, with their C^{α} positions being superimposable to within an r.m.s.d. of 0.4 Å. Each subunit is a small, single-domain protein with the conserved fold composed of a four-stranded antiparallel β-sheet with five connecting α-helices (Figure 4B). The sequence of NDPK is highly conserved in both eukaryotic and prokaryotic enzymes, with a minimal pairwise homology of

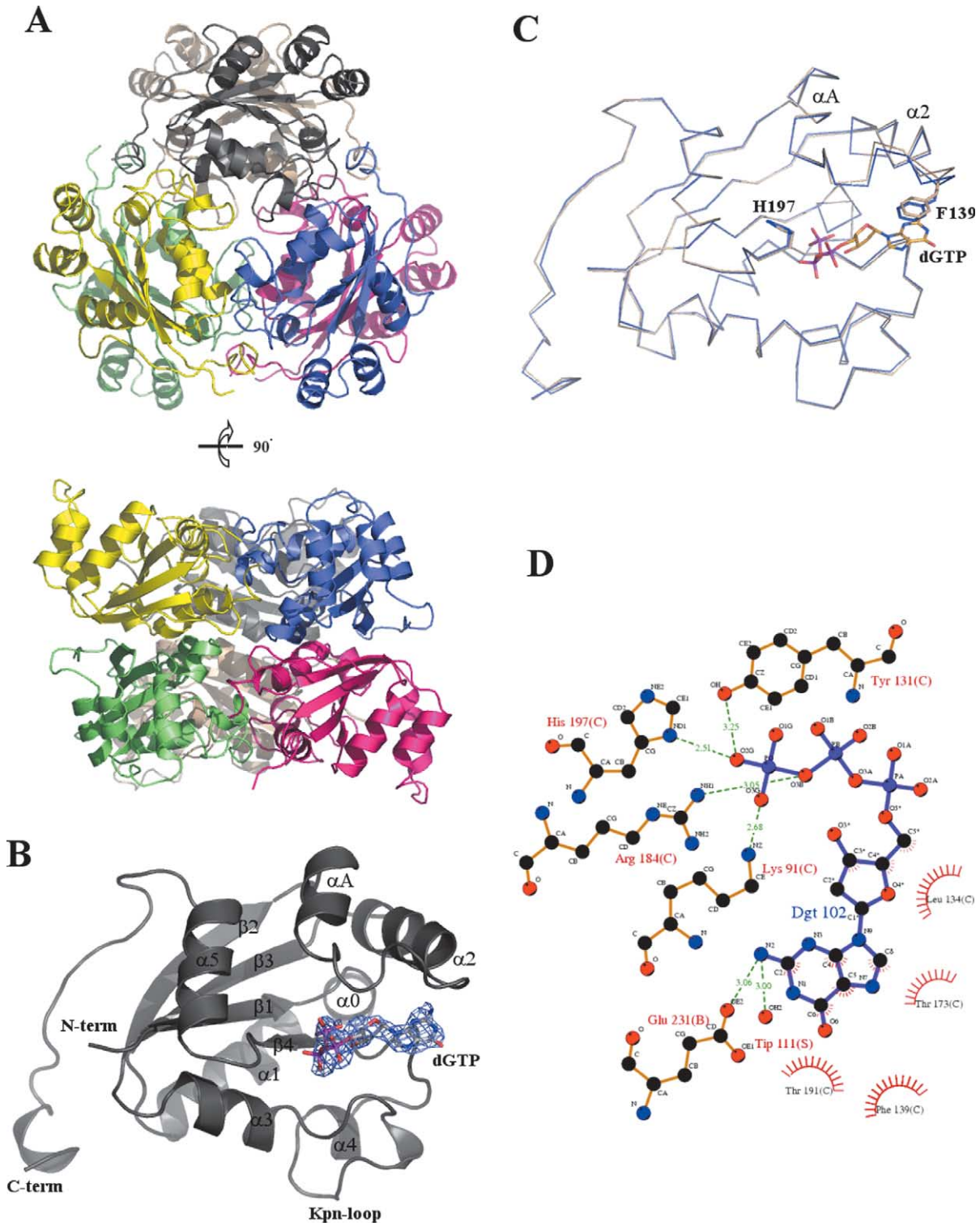

Figure 4. Structure of *Arabidopsis thaliana* NDPK2. A, Ribbon diagram of an NDPK2 hexamer viewed along the 3-fold axis. The hexamer rotated 90° perpendicular to the 3-fold axis is shown on the right. B, Ribbon diagram showing an NDPK2 monomer with a ball-and-stick model showing the bound dGTP. $2F_o - F_c$ map of the dGTP molecule is shown. C, Superposition of C^{α} traces of the apo and nucleotide-bound structures. The apo form is colored in wheat and the dGTP bound form in blue. The Figures were made using PyMOL (http://pymol.sourceforge.net). D, Illustration of amino-acid contacts to the dGTP ligand in the active site. Hydrogen bonds and salt-bridges are shown as broken green lines and van der Waals contacts as bent red combs. The Figure was produced using LIGPLOT.[54]

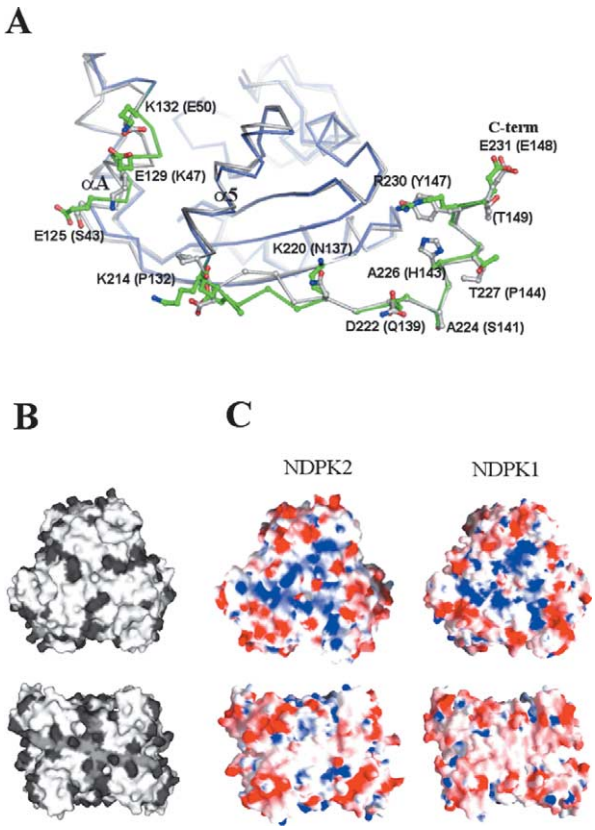

Figure 5. Structure comparison of NDPK1 and NDPK2. A, C^{α} superposition of NDPK1 and NDPK2. NDPK2 is colored in blue and the variable residues in the C-terminal extension and helix αA are colored in green. NDPK1 is colored in wheat and the residue numbers are shown in parentheses. B, Side-chains of 20 variable residues in each subunit, which are indicated by filled triangles in Figure 1C, are colored in black. Backbones of the C-terminal 19 residues of each NDPK2 subunit are colored in gray. C, Electrostatic surface models of NDPK1 and NDPK2. The upper row shows the top view of the 3-fold axis of the hexamers; the lower row shows the side-view of hexamers. Electrostatic surface models were drawn using the program GRASP.[55]

44%. All of the sequences of the eukaryotic enzymes can be aligned optimally, with no insertion longer than one residue. On the other hand, the C-terminal 20 residues are less well conserved than the preceding N-terminal sequences.

The structures of apo and dGTP-bound NDPK2 superimpose with an overall r.m.s.d of 0.48 Å, indicating there is little overall conformational change upon nucleotide binding (Figure 4C). A pair of surface helices (αA and α2) and the loop connecting them in the nucleotide-binding site display the largest structural change with a movement of 0.96 Å (Phe139), which accounts for most of the conformational change elicited by nucleotide binding. The geometry of dGTP bound in the active site and the slight conformational change of helices αA and α2 were consistent with the previously solved structures of nucleotide-bound NDPKs (Figure 4D).[8,34,35]

When the structure of NDPK2 (residues 83–231) was compared with that of NDPK1, all common C^{α} atoms were superimposable within an r.m.s.d. of 0.76 Å, which is indicative of the high degree of structural conservation of these enzymes. The highest conformational difference between the isoforms is in the helices αA and α2, which have the greatest conformational flexibility to accommodate the nucleotide substrates. NDPK1 and NDPK2 share almost identical secondary and tertiary structures over all residues except the C-terminal loop following helix α5. NDPK2 has a single-residue insertion (K214) at the C-terminal extension resulting in different conformation of the loop residues spanning 214 to 218 (Figure 5A). The structure comparison of C-terminal extensions indicates that, although the backbone structures beyond residue 219 are almost identical, exposed side-chains in the extension are unique for each isoform.

Structural basis of the specific interaction of NDPK2 and phytochrome

NDPK2 shares 72% to 75% similarity with NDPK1 and NDPK3, respectively; the difference being mainly in the C-terminal 30 residues (Figure 1C), and domain-swap results showed that the C-terminal region is important for the phytochrome binding and activation. Residues strictly conserved among NDPK isoforms are located mostly in the buried subunit interface and active site, indicating that the ternary structures of the three isoforms are essentially identical. A surface model of NDPK2 shows that the variable residues

of the C-terminal extension and helix αA (colored in dark gray) are concentrated mainly on the equatorial surface of the NDPK hexamer (Figure 5B). Electrostatic surface representation of the structures of NDPK1 and NDPK2 and the homology model of NDPK3 shows that the three isoforms share common electrostatic surfaces on the upper side of the hexamer, where the active sites are located, while the distribution of electrostatic charges on the equatorial surface of the hexamers is distinct for each isoform (Figure 5C). This suggests that it is the variable C-terminal extension displaying a unique surface characteristic of each isoform that might mediate the specific interaction between NDPK2 and phytochrome.

Discussion

The present study provides the first information on the structure of NDPK from a plant system and the structural basis for the interaction between NDPK2 and the phytochromes involved in regulating plant photomorphogenesis. Notably, the interaction between phyA and NDPK2 was enhanced substantially in the presence of diphospho- or triphosphonucleoside; thus, the binding of nucleotide to the active site of NDPK2 optimizes the enzyme's interaction with phytochrome. The Pfr form of phyA does not differentiate between purine and pyrimidine nucleotides, or between NDPs and NTPs, as both dCDP and ATP enhanced the NDPK2–phytochrome interaction. Upon nucleotide binding, there was also a conformational change affecting surface helices αA and α2. Although the movement was limited to 1 Å or less, this could contribute to the increased affinity between NKPK2 and phytochrome. The base in the structure is located in a cleft near the protein surface and makes only non-polar interactions, except with Glu231 (Figure 4D). Unlike the α and β-phosphate groups, which are partly accessible to the solvent, the ribose ring is almost completely buried in the active site. This suggests that phytochrome may directly recognize the di-phosphoryl group accessible from the surface, or the conformational change caused by nucleotide binding may enable the phytochrome to recognize it.

Using *in vitro* binding assays, we found that the regulatory domain of phyA (residues 574–957) is critical for the interaction with NDPK2. Phytochromes have two major structural and functional regions:[30,36] an N-terminal signal-sensing domain, where chromophore binding and light perception occur, and a C-terminal signal-transducing domain, which contains two PAS-related domains and a histidine kinase-related domain.[30] The importance of the C-terminal half of plant phytochromes is highlighted by numerous missense mutations affecting this portion of the protein.[36] The PAS domains comprise the regulatory domain of phytochromes (residues 623–778 in oat phyA) and are required for interaction with phytochrome signaling partners.[37–39] Our finding that the C-terminal region of phyA is responsible for the interaction with NDPK2 is consistent with our recent model of Pr→Pfr phototransformation.[30,37] Upon illumination, phytochromes are transformed from the Pr to the Pfr form accompanying a conformational change. The N-terminal extension region of phyA goes from a random coil to an amphiphilic α-helix that interacts with the Pfr form of the chromophore[31,40] and two tryptophan residues in the C-terminal regulatory domain become exposed.[41] On the basis of these results, it has been proposed that the N-terminal extension interacts with the regulatory C-terminal domain in the Pr form ("switched off" conformation).[42] Upon Pr→Pfr phototransformation ("switched on" conformation), the N-terminal extension is withdrawn due to a conformational change, exposing the regulatory domain and enabling interaction with phytochrome signal transducer(s), thereby initiating the signaling cascade.

The structure comparison and sequence alignment of NDPK1, NDPK2, and NDPK3 showed the main differences among the three NDPK isoforms to reside in the C-terminal extension. The 19 variable C-terminal residues are exposed on the equatorial surface of the NDPK hexamer and occupy 21.5% of the hexamer's surface area. Structural comparison of NDPK1 and NDPK2 further revealed that the distributions of electrostatic potentials on their equatorial surfaces differ, suggesting that the variable C-terminal extension is central to the specific function of each NDPK isoform. Our domain-swap experiments provide the supporting evidence for the crucial role of the variable C-terminal extension for the interaction with and activation by phytochrome. Thus, whereas the N-terminal region provides the framework for the enzyme's conserved catalytic activity, the C-terminal extension of the respective NDPK isoforms provides specific electrostatic and hydrophobic characteristics that determine protein binding and selectivity.

The structures and biochemical characteristics of human NDPK-A and NDPK-B led to similar speculation about the involvement of unique surface features in their respective cellular functions.[12,19] Although their amino acid sequences share a high degree of similarity (88% identity), the two proteins have distinct regulatory functions: NDPK-A suppresses metastasis, while NDPK-B acts as a transcription factor regulating *c-myc* oncogene expression.[21] Using site-directed mutagenesis, NDPK-B was shown to have a sequence-dependent DNA-binding surface at the equator of the hexamer and a covalent DNA-binding site within the nucleotide-binding site.[17–19] On the other hand, NDPK-A, which has DNase activity, forms complexes with SET, pp32, HMG-2, and Ape1 in order to function in DNA repair or GzmA-mediated cell death.[22] This implies that NDPK-A possesses a specific surface for the protein–protein interaction. In each of these cases, a contribution by the variable C-terminal extension located in the equatorial surface of hexamers to their

specific functions through the protein–protein interaction cannot be excluded.

It is intriguing that the diverse regulatory functions of these proteins coexist along with highly conserved catalytic activity and structure. In that regard, the available crystal structures of NDPKs having diverse cellular functions do not show significant difference in their backbone structures to account for their specific functions by unique conformational changes, except for the concerted movement of active-site helices upon nucleotide binding.[34] Therefore, diverse regulatory roles of NDPKs might be mediated by the interaction with the various binding partners rather than the unique functions of NDPK themselves. Perhaps the specific regulatory function of each NDPK is related to a unique distribution of residues on the surface of the conserved enzyme skeleton.

Within *A. thaliana*, NDPK2 appears to mediate signaling leading to cotyledon unfolding and greening responses elicited by light and phytochromes.[27] Zimmerman *et al*. showed that NDPK2 may serve as a transcription factor in UV-B light signaling.[24] Until now, the downstream signaling pathway of NDPK2 is not known with certainty. In the present study, we obtained new evidence of the regulation of the phytochrome–NDPK2 interaction by nucleotides. However, how the nucleotide-dependent interaction of the proteins is involved in the modulation of phytochrome signaling remains unclear. NDPKs are distributed ubiquitously and di- or trinucleotides are always present in living cells. The amount of nucleotide present is related to the energy charge needed for cellular metabolism and function. Therefore, a pool of NDPK2 enzyme might be loaded dynamically with nucleotides in some proportion to the available nucleotides, after which the nucleotide-bound enzyme, serving as an upstream light signal transducer, may modulate a specific interaction with phytochromes. Because only the Pfr form of phytochromes interacts with nucleotide-bound NDPK2 to activate the enzymatic activity, which signals the presence of light to which plant cells respond, it is possible that phytochrome-mediated light signaling is transduced through the modulation of NDPK2 by the red/far-red photoreceptor, possibly followed by specific activation of signaling component(s); e.g. small molecular mass and/or heterotrimeric G-proteins.

Materials and Methods

Purification of NDPKs

Recombinant NDPK2 lacking a signal sequence (residues 80–231) from *A. thaliana* was subcloned into pGEX 4T vector (Pharmacia) using primers:

5′-CTCGGATCCATGGAGGACGTTGAGGAGACT TAC-3′ (BamHI, forward)

and:

5′-CGGAATTCTCACTCCCTTAGCCATGTAGC-3′ (EcoRI, backward)

as were full-length NDPK1 (1–149) and NDPK3 (88–238) using primers:

5′-CTCGGATCCATGGAGCAAACTTTTATTATGAT C-3′ (BamHI, forward)

and:

5′-CGGAATTCTCAAGTTTCATAGACCCAAGGGT G-3′ (EcoRI, backward)

for the former and:

5′-CTCGGATCCATGGAACGAACTTTTATTGCTAT C-3′ (BamHI, forward)

and:

5′-CGGAATTCTCAGTTGTCACCATAGAGCCACTT C-3′ (EcoRI, backward)

for the latter. For the domain-swap mutants:

5′-CTCGGTACCAGGCTCAGAAGCTGCTG-3′ (KpnI, backward)

and:

5′-CTCGGTACCATCCGTGGGGACTTTGCTATTG-3′ (KpnI, forward)

were used for N and C-terminal domains of NDPK1, respectively. KpnI was used for the swap. Primers:

5′-CTCGGTACCAGGTTCAGCTTGAAGC-3′ (KpnI, backward)

and:

5′-CTCGGTACCATAAGAG GGAGATCTTGCTGTG C-3′ (KpnI, forward)

were used for N and C-terminal domains of NDPK2, respectively. NDPK proteins with a cleavable GST tag were expressed in *Escherichia coli* strain BL21 (DE3). The bacterial cells were induced at 37 °C for four hours with 1 mM isopropyl β-D-thiogalactopyranoside (IPTG) and then harvested by centrifugation at 4500*g* for 20 minutes. The cells were resuspended in PBS and lysed by sonication, after which the lysate was centrifuged at 16,000*g* for 30 minutes. The resultant supernatant was applied to a glutathione-Sepharose 4B affinity column pre-equilibrated with PBS, after which the column was washed with ten bed volumes of lysis buffer. The GST fusion protein bound to the column was eluted with a buffer of 10 mM glutathione and 50 mM Tris–HCl (pH 8.0). GST tags were cleaved from NDPKs by treatment with thrombin for two days at room temperature. The samples were then purified by size-exclusion chromatography using a Superdex 200 column (Pharmacia Biotech) pre-equilibrated with a buffer of 10 mM Tris–HCl (pH 8.0), 50 mM NaCl after which the fractions containing NDPKs were collected. GST protein remaining after the size-exclusion chromatography was removed by glutathione-Sepharose 4B affinity chromatography. Fractions containing NDPKs were then collected and concentrated to 4–5 mg/ml.

Purification of phytochromes

Native 124 kDa phytochrome A (phyA) was purified in the Pfr form from 3.5-days old etiolated oat seedlings (*Avena sativa* L.) as described.[43] The specific absorbance ratio of native phytochrome preparations was over 1.00. To express recombinant phytochrome proteins, the oat phyA gene from pFY122[44] was amplified using primers:

5′-CTCGGATCCACCATGGAGCAAACTTTTATTAT GATC-3′ (BamH1, forward)

and:

5′-TCGCGTCGACCTTGTCCCATTGCTGTTGGAGC-3′ (SalI, backward).

The amplified PCR product was subcloned into the pASK75 vector (Biometra) to add a nucleotide sequence encoding the streptavidin affinity-tag (strep-tag) at the 3′

end of the oat phyA gene and then subcloned into the BamHI/NotI sites of the *Pichia* expression vector pPIC3.5K (Invitrogen). Note that prior to subcloning the phytochrome genes, the pASK75 vector was modified so that it contained a NotI restriction site at the end of the strep-tag for the compatibility with the *Pichia* expression vector pPIC3.5K. The gene encoding a phyA mutant lacking the N-terminal 65 residues (AΔ65, residues 66–1129) was amplified by PCR using the forward primer:

5′-CGGGATCCACCATGGTCATAGCCTACTTACAG CAC-3′.

For a phyA deletion mutant (A957, residues 1–957), the backward primer used was:

5′-TCGCGTCGACCTTCGGTGATGCTATCTTGATCC-3′.

Genes encoding the N-terminal chromophore-binding domain (A407, residues 1–407) and the C-terminal domain (AC, residues 574–1129) were amplified using the primers:

5′-CTCCATATGGAGCAAACTTTTATTATGATC-3′ (NdeI, forward)

and:

5′-CGCCCGGGCTGTTTCTCTAATTCAAACTCC-3′ (SmaI, backward)

for A407 and:

5′-CTCCATATGGATGCTATTCATTCATTGC-3′ (NdeI, forward)

and:

5′-CGCCCGGGTCATTGTCCCATTGCTGTTGGAGC-3′ (SmaI, backward)

for AC. The A407 and AC constructs were subcloned into the NdeI/SmaI sites of pTYB2 (New England Biolab), expressed in *E. coli* strain ER2566, and purified by chitin affinity chromatography, according to the manufacturer's recommendations (New England Biolab).

Pichia cells were transformed with pPIC3.5K vectors (Invitrogen) containing the phytochrome genes using a Micropulser™ Electroporator (Bio-Rad) according to the manufacturer's recommendations, after which the expressed recombinant phytochromes were purified by streptavidin affinity chromatography (Sigma-Genosys). For the preparation of holophytochromes, phytochromobilin was extracted from the red alga *Porphyridium cruentum* by methanolysis and purified by chromatography as described.[45] Crude extracts were prepared from harvested *Pichia* cells by breaking cells with a homogenizer (Nihonseiki Kaisha Ltd) after freezing them in liquid nitrogen. Apophytochromes were precipitated by adding 0.23 g/l of ammonium sulfate and then resuspended in 100 mM Tris–HCl (pH 7.8), 1 mM EDTA. Holophytochromes were prepared by adding phytochromobilin chromophores dissolved in DMSO to the apoproteins to a final concentration of 20 μM, after which the mixture was incubated for one hour on ice. Direct addition of chromophores to the ammonium sulfate fraction resulted in better reconstitution of holoproteins than addition to purified apoproteins. After removing the free chromophores by dialysis, the holophytochromes were purified by streptavidin affinity chromatography. To confirm the assembly of holophytochromes, Zn^{2+} fluorescence assays (Zn blot) were carried out as described.[42] Briefly, the proteins were subjected to SDS-PAGE, after which the gels were soaked in 150 mM Tris–HCl (pH 7.0), 20 mM zinc acetate for five to 30 minutes at room temperature with gentle shaking. The blots were then visualized under UV light (312 nm). Either the Pr or Pfr form of phytochromes was prepared by irradiating the samples with red or far-red light for two minutes before the start of the experiment. A fiber-optic illuminator system (Cole-Parmer) equipped with 656 nm and 730 nm interference filters (Oriel) was used as a light source. The light intensity was 8 W/m^2 for red light and 6 W/m^2 for far-red light.

In vitro binding assays

Purified phytochrome (10 μg) in either Pr or Pfr form and 20 μg of GST-NDPK2 were incubated for 30 minutes at 4 °C in TBS buffer (50 mM Tris–HCl (pH 7.5), 150 mM NaCl) containing protease inhibitors with or without 1 mM nucleotides. For immunoprecipitation, anti-oat phyA mAb[46] was added to the reaction mixtures, after which the mAb/phytochrome complexes were recovered by incubation with 0.1 volume of protein A/G beads (Oncogene) for an additional 30 minutes with occasional mixing and then centrifugation. For pull-down assays, glutathione affinity resin washed with PBS was added to the mixtures. The beads were then washed five times by TBS buffer containing 0.1% (v/v) NP-40. The attached proteins were solubilized by boiling for three minutes in SDS sample buffer and the proteins were resolved on SDS/10% (w/v) polyacrylamide gels and transferred to a polyvinylidene difluoride (PVDF) membrane (Hybond-P, Amersham Pharmacia Biotech). The membrane was then incubated for two hours with oat anti-phyA or anti-NDPK2[26] mAb and developed using an ECL™ Western blot analysis system (Amersham).

NDPK2 γ-phosphate exchange activity assay

NDPK2 γ-phosphate exchange activity was measured essentially as described but with minor modifications.[27] The assay buffer was 50 mM Tris–HCl (pH 7.5), 5 mM $MgCl_2$, 3 mM phosphoenolpyruvate, 2 mM ATP, 0.3 mM NADH, five units of pyruvate kinase (PK), five units of lactate dehydrogenase (LDH), and 1 mM dCDP. The reaction was initiated by adding 3 nM NDPK2. NDPK2 activity was measured by monitoring the LDH-PK-coupled NADH decrease at 340 nm. The phytochrome effect was examined by incubating a mixture of native oat phyA and NDPK2 under illumination of red light (660 nm, Pfr form) or far-red light (730 nm, Pr form) for eight minutes and measuring NDPK2 activity with different concentrations of phytochromes.

Crystallization

Arabidopsis NDPK1 was crystallized at room temperature (20(±1) °C) using the hanging-drop, vapor-diffusion method. Crystals were grown on a siliconized cover-slip by equilibrating a mixture containing 2 μl of protein solution (6 mg/ml protein in 10 mM Tris–HCl (pH 8.0), 50 mM NaCl) and an equal volume of well solution (100 mM Tris–HCl (pH 8.0), 19% (w/v) PEG 4000, 0.2 M $MgCl_2$) against 1.0 ml of well solution. Crystals appeared within a week and grew to dimensions of 0.1 mm × 0.1 mm × 0.2 mm, and were flash-frozen by direct transfer to Pratone-N cryoprotectant solution (Hampton Research). NDPK2 crystals were grown on a siliconized cover-slip by equilibrating a mixture containing 2 μl of protein solution (4.2 mg/ml protein in 10 mM Tris–HCl (pH 8.0), 50 mM NaCl) and an equal volume of well solution (100 mM Hepes–NaOH (pH 7.0), 2.4 M ammonium sulfate) against 1.0 ml of well solution. Crystals appeared after one week, grew to dimensions of 0.1 mm × 0.2 mm × 1.0 mm, and were flash-frozen

using Pratone-N cryoprotectant solution (Hampton Research). Crystals of the dGTP-bound form of NDPK2 were grown using the identical crystallization conditions, except the protein solution contained 10 mM dGTP.

Crystallographic analysis

A native data set of the apo NDPK2 crystal was collected at $\lambda = 1.000$ Å from a single frozen crystal with an ADSC Quantum Q210 CCD detector at beamline AR NW12 at the Photon Factory, Japan. The data set was processed and scaled using HKL2000 packages[47] and then handled with the CCP4 program suite.[48] The structure was solved by molecular replacement with AMoRe[49] using a hexameric model of human NDP kinase (PDB id 1JXV). The resultant map, showing a hexamer in an asymmetric unit, was readily interpretable. Model building was then carried out using the program O,[50] after which the structure was refined using the program CNS.[51] The final crystallographic *R* value calculated using data from 50 Å to 1.8 Å, was 21.3% (R_{free} 24.1%). The stereochemistry of the model was analyzed with PROCHECK.[52] It showed that Ile195 in each of three subunits was in a disallowed region; Ile195 is located at the center of a tight Kpn-loop between helix α4 and strand β4 and they were well defined in the electron density maps.

Data sets for NDPK1 and dGTP-complexed NDPK2 were collected with a MacScience DIP2030b imaging plate at beamline 6B at Pohang Light Source, Pohang, Korea. The data sets were integrated and scaled with HKL and SCALEPACK.[47] To solve the structure of the dGTP-bound form, the structure of apo NDPK2 was used for molecular replacement calculation. The electron density map obtained after several refinement steps showed clearly the bound dGTP in molecule C and dGDP in molecule A. However, no nucleotide was observed in molecule B or E due to obstruction of the active site by crystallographic packing interactions between the hexamers. The active sites of molecules D and F showed weak electron densities of phosphate groups, which were not included in the final model. We concluded that because the enzyme used for crystallization was catalytically active, the dGDP and inorganic phosphate products were incorporated into the structure. The final model of the dGTP and dGDP-bound structure was refined to the crystallographic *R* value of 20.7% (R_{free} 28.2%). The structure of NDPK1 was solved by molecular replacement as described above and refined to the free *R* value of 28.1%. Data collection and refinement statistics are summarized in Table 1.

Table 1. Data collection and refinement statistics

	Data set		
	Apo NDPK2	NDPK2 dGTP complex	Apo NDPK1
A. *Data collection*			
X-ray source	PF-AR NW12	PAL 6B	PAL6B
Wavelength	1.000	1.127	1.127
Space group	$P2_12_12_1$	$P2_12_12_1$	$P2_12_12_1$
Unit cell parameters			
a (Å)	69.4	69.0	73.9
b (Å)	108.9	108.5	96.3
c (Å)	119.3	118.3	134.7
Resolution (Å)	50–1.8	50–2.6	50–2.4
No. observations	680,641	147,357	253,561
Unique reflections	84,434	27,023	36,843
R_{sym}[a] (%)	6.8 (37.3)[b]	12.3 (39.4)	7.2 (31.8)
Data coverage total (%)	99.9 (98.3)[b]	95.9 (91.4)	96.4 (99.6)
B. *Data refinement*			
R_{cryst}[c] total (%)	21.3	20.7	23.0
R_{free}[d] total (%)	24.1	28.2	28.1
r.m.s.d from ideality			
Bond lengths (Å)	0.005	0.007	0.008
Bond angles (deg.)	1.3	1.4	1.3
Average *B*-value (Å^2)	21.6	19.6	42.9

[a] $R_{sym} = \sum |\langle I \rangle - I| / \sum \langle I \rangle$.
[b] Values in parentheses relate to the highest-resolution shells (apo NDPK2, 1.83–1.80 Å; dGTP-complexed NDPK2, 2.69–2.60 Å; NDPK1, 2.44–2.40 Å).
[c] $R_{cryst} = \sum ||F_o| - |F_c|| / \sum |F_o|$.
[d] R_{free} calculated using 5% of all reflections excluded from the refinement stages.

Atomic coordinates

The atomic coordinates and structure factors of NDPK1, NDPK2, and dGTP-complexed NDPK2 have been deposited in the RCSB Protein Data Bank under entry codes 1U8W, 1S57, and 1S59, respectively.

Acknowledgements

We thank Professor N. Sakabe, Dr M. Suzuki, and Dr N. Igarashi for their kind support with X-ray data collection at beamline AR NW12 at the Photon Factory, Tsukuba, Japan. Parts of this study were carried out at beamline 6B at the Pohang Accelerator Laboratory. This work was supported by Korea Kumho Petrochemical Co., Ltd. (KKPC, publication no. 71), grants from the National Research Laboratory/KISTEP, BioGreen 21 program of Rural Development Administration (RDA) (to P.-S.S.), Crop Functional Genomics Center of the 21st Century Frontier Research Program by the MOST and RDA (code M101KG010001-03K0701-02910), and the KOSEF/MOST to the Environmental Biotechnology National Core Research Center (NCRC) (to J.-I.K. and P.-S.S; grant R15-2003-012-01003-0).

References

1. Parks, R. E. & Agarwal, R. P. (1973). Nucleoside diphosphokinases. In *The Enzymes* (Boyer, P. D., ed.), vol. 8, pp. 307–333, Academic Press, New York.
2. Morera, S., Chiadmi, M., LeBras, G., Lascu, I. & Janin, J. (1995). Mechanism of phosphate transfer by nucleoside diphosphate kinase: X-ray structures of the phosphohistidine intermediate of the enzymes from *Drosophila* and *Dictyostelium*. *Biochemistry*, **34**, 11062–11070.
3. Xu, Y. W., Morera, S., Janin, J. & Cherfils, J. (1997). AlF3 mimics the transition state of protein phosphorylation in the crystal structure of nucleoside diphosphate kinase and MgADP. *Proc. Natl Acad. Sci. USA*, **94**, 3579–3583.
4. Gonin, P., Xu, Y., Milon, L., Dabernat, S., Morr, M., Kumar, R. *et al*. (1999). Catalytic mechanism of

nucleoside diphosphate kinase investigated using nucleotide analogues, viscosity effects, and X-ray crystallography. *Biochemistry*, **38**, 7265–7272.
5. Admiraal, S. J., Schneider, B., Meyer, P., Janin, J., Veron, M., Deville-Bonne, D. & Herschlag, D. (1999). Nucleophilic activation by positioning in phosphoryl transfer catalyzed by nucleoside diphosphate kinase. *Biochemistry*, **38**, 4701–4711.
6. Dumas, C., Lascu, I., Morera, S., Glaser, P., Fourme, R., Wallet, V. *et al*. (1992). X-ray structure of nucleoside diphosphate kinase. *EMBO J.* **11**, 3203–3208.
7. Chiadmi, M., Morera, S., Lascu, I., Dumas, C., Le Bras, G., Veron, M. & Janin, J. (1993). Crystal structure of the Awd nucleotide diphosphate kinase from Drosophila. *Structure*, **1**, 283–293.
8. Williams, R. L., Oren, D. A., Munoz-Dorado, J., Inouye, S., Inouye, M. & Arnold, E. (1993). Crystal structure of *Myxococcus xanthus* nucleoside diphosphate kinase and its interaction with a nucleotide substrate at 2.0 Å resolution. *J. Mol. Biol.* **234**, 1230–1247.
9. Webb, P. A., Perisic, O., Mendola, C. E., Backer, J. M. & Williams, R. L. (1995). The crystal structure of a human nucleoside diphosphate kinase, NM23-H2. *J. Mol. Biol.* **251**, 574–587.
10. Abdulaev, N. G., Karaschuk, G. N., Ladner, J. E., Kakuev, D. L., Yakhyaev, A. V., Tordova, M. *et al*. (1998). Nucleoside diphosphate kinase from bovine retina: purification, subcellular localization, molecular cloning, and three-dimensional structure. *Biochemistry*, **37**, 13958–13967.
11. Milon, L., Meyer, P., Chiadmi, M., Munier, A., Johansson, M., Karlsson, A. *et al*. (2000). The human nm23-H4 gene product is a mitochondrial nucleoside diphosphate kinase. *J. Biol. Chem.* **275**, 14264–14272.
12. Min, K., Song, H. K., Chang, C., Kim, S. Y., Lee, K. J. & Suh, S. W. (2002). Crystal structure of human nucleoside diphosphate kinase A, a metastasis suppressor. *Proteins: Struct. Funct. Genet.* **46**, 340–342.
13. Chen, Y., Morera, S., Mocan, J., Lascu, I. & Janin, J. (2002). X-ray structure of *Mycobacterium tuberculosis* nucleoside diphosphate kinase. *Proteins: Struct. Funct. Genet.* **47**, 556–557.
14. Chen, C.-J., Liu, M.-Y., Chang, T., Chang, W.-C., Wang, B.-C. & Le Gall, J. (2003). Crystal structure of a nucleoside diphosphate kinase from *Bacillus halodenitrificans*: coexpression of its activity with a Mn-superoxide dismutase. *J. Struct. Biol.* **142**, 247–255.
15. Janin, J., Dumas, C., Morera, S., Xu, Y., Meyer, P., Chiadmi, M. & Cherfils, J. (2000). Three-dimensional structure of nucleoside diphosphate kinase. *J. Bioenerg. Biomembr.* **32**, 215–225.
16. Lascu, L., Giartosio, A., Ransac, S. & Erent, M. (2000). Quaternary structure of nucleoside diphosphate kinases. *J. Bioenerg. Biomembr.* **32**, 227–236.
17. Postel, E. H., Abramczyk, B. A., Gursky, S. K. & Xu, Y. (2002). Structure-based mutational and functional analysis identify human NM23-H2 as a multifunctional enzyme. *Biochemistry*, **41**, 6330–6337.
18. Postel, E. H., Abramczyk, B. M., Levit, M. N. & Kyin, S. (2000). Catalysis of DNA cleavage and nucleoside triphosphate synthesis by NM23-H2/NDP kinase share an active site that implies a DNA repair function. *Proc. Natl Acad. Sci. USA*, **97**, 14194–14199.
19. Postel, E. H., Weiss, V. H., Beneken, J. & Kirtane, A. (1996). Mutational analysis of NM23-H2/NDP kinase identifies the structural domains critical to recognition of a c-myc regulatory element. *Proc. Natl Acad. Sci. USA*, **93**, 6892–6897.
20. Agou, F., Raveh, S., Mesnildrey, S. & Veron, M. (1999). Single strand DNA specificity analysis of human nucleoside diphosphate kinase B. *J. Biol. Chem.* **274**, 19630–19638.
21. Rosengard, A. M., Krutzsch, H. C., Shearn, A., Biggs, J. R., Barker, E., Margulies, I. M. *et al*. (1989). Reduced Nm23/Awd protein in tumour metastasis and aberrant *Drosophila* development. *Nature*, **342**, 177–180.
22. Fan, Z., Beresford, P. J., Oh, D. Y., Zhang, D. & Lieberman, J. (2003). Tumor suppressor NM23-H1 is a granzyme A-activated DNase during CTL-mediated apoptosis, and the nucleosome assembly protein SET is its inhibitor. *Cell*, **112**, 659–672.
23. Escorbar-Galvis, M. L., Marttila, S., Håkansson, G., Forsberg, J. & Knorpp, C. (2001). Heat stress response in pea involves interaction of mitochondrial nucleoside diphosphate kinase with a novel 86-kilodalton protein. *Plant Physiol.* **126**, 69–77.
24. Zimmermann, S., Baumann, A., Jaekel, K., Marbach, I., Engelberg, D. & Frohnmeyer, H. (1999). UV-responsive genes of *Arabidopsis* revealed by similarity to the Gcn4-mediated UV response in yeast. *J. Biol. Chem.* **274**, 17017–17024.
25. Pan, L., Kawai, M., Yano, A. & Uchimiya, H. (2000). Nucleoside diphosphate kinase required for coleoptile elongation in rice. *Plant Physiol.* **122**, 447–452.
26. Moon, H., Lee, B., Choi, G., Shin, D., Prasad, D. T., Lee, O. *et al*. (2003). NDP kinase 2 interacts with two oxidative stress-activated MAPKs to regulate cellular redox state and enhances multiple stress tolerance in transgenic plants. *Proc. Natl Acad. Sci. USA*, **100**, 358–363.
27. Choi, G., Yi, H., Lee, J., Kwon, Y. K., Soh, M. S., Shin, B. *et al*. (1999). Phytochrome signalling is mediated through nucleoside diphosphate kinase 2. *Nature*, **401**, 610–613.
28. Kendrick, R. E. & Kronenberg, G. H. M. (1994). *Photomorphogenesis in Plants* (2nd edit.). Kluwer Academic Publishers, Dordrecht.
29. Quail, P. H., Boylan, M. T., Parks, B. M., Short, T. W., Xu, Y. & Wagner, D. (1995). Phytochromes: photosensory perception and signal transduction. *Science*, **268**, 675–680.
30. Kim, J.-I., Kozhukh, G. V. & Song, P.-S. (2002). Phytochrome-mediated signal transduction pathways in plants. *Biochem. Biophys. Res. Commun.* **298**, 457–463.
31. Deforce, L., Tokutomi, S. & Song, P.-S. (1994). Phototransformation of pea phytochrome A induces an increase in alpha-helical folding of the apoprotein: comparison with a monocot phytochrome A and CD analysis by different methods. *Biochemistry*, **33**, 4918–4922.
32. Wu, S. H. & Lagarias, J. C. (2000). Defining the bilin lyase domain: lessons from the extended phytochrome superfamily. *Biochemistry*, **39**, 13487–13495.
33. Yeh, K. C. & Lagarias, J. C. (1998). Eukaryotic phytochromes: light-regulated serine/threonine protein kinases with histidine kinase ancestry. *Proc. Natl Acad. Sci. USA*, **95**, 13976–13981.
34. Cherfils, J., Morera, S., Lascu, I., Veron, M. & Janin, J. (1994). X-ray structure of nucleoside diphosphate kinase complexed with thymidine diphosphate and Mg^{2+} at 2 Å resolution. *Biochemistry*, **33**, 9062–9069.
35. Morera, S., Lacombe, M. L., Xu, Y., LeBras, G. & Janin, J. (1995). X-ray structure of human nucleoside diphosphate kinase B complexed with GDP at 2 Å resolution. *Structure*, **3**, 1307–1314.

36. Quail, P. H., Boylan, M. T., Parks, B. M., Short, T. W., Xu, Y. & Wagner, D. (1995). Phytochromes: photosensory perception and signal transduction. *Science*, **268**, 675–680.
37. Park, C.-M., Bhoo, S.-H. & Song, P.-S. (2000). Interdomain crosstalk in the phytochrome molecules. *Semin. Cell Dev. Biol.* **11**, 449–456.
38. Quail, P. H. (2000). Phytochrome-interacting factors. *Semin. Cell Dev. Biol.* **11**, 457–466.
39. Genick, U. K. & Chory, J. (2000). Red light sensing in plants. *Curr. Biol.* **10**, R651–R654.
40. Parker, W., Partis, M. & Song, P.-S. (1992). N-terminal domain of Avena phytochrome: interactions with sodium dodecyl sulfate micelles and N-terminal chain truncated phytochrome. *Biochemistry*, **31**, 9413–9420.
41. Wells, T. A., Nakazawa, M., Manabe, K. & Song, P.-S. (1994). A conformational change associated with the phototransformation of Pisum phytochrome A as probed by fluorescence quenching. *Biochemistry*, **33**, 708–712.
42. Berkelman, T. R. & Lagarias, J. C. (1986). Visualization of bilin-linked peptides and proteins in polyacrylamide gels. *Anal. Biochem.* **156**, 194–201.
43. Lapko, V. N. & Song, P.-S. (1995). A simple and improved method of isolation and purification for native oat phytochrome. *Photochem. Photobiol.* **62**, 194–199.
44. Boylan, M. T. & Quail, P. H. (1989). Oat phytochrome is biologically active in transgenic tomatoes. *Plant Cell*, **1**, 765–773.
45. Beale, S. I. & Cornejo, J. (1991). Biosynthesis of phycobilins. 3(Z)-phycoerythrobilin and 3(Z)-phycocyanobilin are intermediates in the formation of 3(E)-phycocyanobilin from biliverdin IX alpha. *J. Biol. Chem.* **266**, 22333–22340.
46. Cordonnier, M.-M., Smith, C., Greppin, H. & Pratt, L. H. (1983). Production and purification of monoclonal antibodies to *Pisum* & *Avena* phytochrome. *Planta*, **158**, 369–376.
47. Otwinowski, Z. & Minor, W. (1997). Processing of X-ray diffraction data collected in oscillation mode. *Methods Enzymol.* **276**, 307–326.
48. Collaborative Computational Project Number 4. (1994). The CCP4 suite: programs for protein crystallography. *Acta Crystallog. sect. D*, **50**, 760–763.
49. Navaza, J. (1994). AMoRe: an atomated package for molecular replacement. *Acta Crystallog. sect. A*, **50**, 157–163.
50. Jones, T. A., Zou, J.-Y., Cowan, S. W. & Kjeldgaard, M. (1991). Improved methods for building protein models in electron density maps and the location of errors in these models. *Acta Crystallog. sect. A*, **47**, 110–119.
51. Brunger, A. T., Adams, P. D., Clore, G. M., DeLano, W. L., Gros, P., Grosse-Kunstleve, R. W. *et al.* (1998). Crystallography & NMR system: a new software suite for macromolecular structure determination. *Acta Crystallog. sect. D*, **54**, 905–921.
52. Laskowski, R. A., MacArthur, M. W., Moss, D. S. & Thornton, J. M. (1993). PROCHECK: a program to check the stereochemical quality of protein structures. *J. Appl. Crystallog.* **26**, 283–291.
53. Thompson, J. D., Gibson, T. J., Plewniak, F., Jeanmougin, F. & Higgins, D. G. (1997). The CLUSTAL_X windows interface: flexible strategies for multiple sequence alignment aided by quality analysis tools. *Nucl. Acids Res.* **25**, 4876–4882.
54. Wallace, A. C., Laskowski, R. A. & Thornton, J. M. (1995). LIGPLOT: a program to generate schematic diagrams of protein-ligand interactions. *Protein Eng.* **8**, 127–134.
55. Nicholls, A., Sharp, K. A. & Honig, B. (1991). Protein folding and association: insights from the interfacial and thermodynamic properties of hydrocarbons. *Proteins: Struct. Funct. Genet.* **11**, 281–296.

Edited by R. Huber

(Received 30 April 2004; received in revised form 17 August 2004; accepted 18 August 2004)